Systematic trends in self-consistent calculations of linear quantum wires

J. Martorell
Departament d'Estructura i Constituents de la Materia, Facultat Física, University of Barcelona, Barcelona 08028, Spain

Hua Wu and D. W. L. Sprung
Department of Physics and Astronomy, McMaster University, Hamilton, Ontario, Canada L8S 4M1
(Received 12 July 1994)

Systematic trends in the properties of a linear split-gate heterojunction are studied by solving iteratively the Poisson and Schrödinger equations for different gate potentials and temperatures. A two-dimensional approximation is presented that is much simpler in the numerical implementation and that accurately reproduces all significant trends. In deriving this approximation, we provide a rigorous and quantitative basis for the formulation of models that assume a two-dimensional character for the electron gas at the junction.

I. INTRODUCTION

The properties of the electron gas formed in gated $Al_xGa_{1-x}As/GaAs$ heterojunctions have been extensively studied in recent years, particularly the quantum phenomena appearing in the transport of electrons under a split gate. Many models that exploit the almost two-dimensional character of the electron wave functions have been developed to explain these properties and describe the behavior of the electrons in these so-called quantum wires. However, to our knowledge, there are only a few examples in the existing literature of fully three-dimensional self-consistent calculations of the electron gas properties in a quantum wire under stationary conditions, and in none of them is a quantitative connection with two-dimensional models discussed. This is the main objective of this work.

The reference calculation for a linear split gate of constant width is that of Laux *et al.*,[1] later extended to a wire of periodically varying width[2] and to quantum dots.[3] Linear split gate devices with somewhat more involved geometry have been considered by Snider *et al.*,[4] by Kerkhoven *et al.*,[5] and more recently by Jovanovic and Leburton[6] and by Wu and Ruden.[7] The calculations of Laux *et al.*[1] have had a considerable impact in the development of models, because they have provided the main theoretical support to certain simplifying assumptions on the profile of the confining walls and corresponding properties of the electron wave functions, used in most discussions of transport in quantum wires. However, the complexity of three-dimensional calculations, which require an iterative solution of the Poisson and Schrödinger equations, has restricted them until now to a few specific cases. In this work we present methods and approximations appropriate for linear split-gate devices which simplify the numerical treatment and therefore allow one to perform more systematic studies and to clarify the physical interpretation of the results.

Extending a method originally proposed by Davies,[8] we determine the potential due to the gates analytically, avoiding the numerical integration of the Poisson equation in the cap and donor layers. Therefore only the potential due to the mutual repulsion between the electrons and, eventually, between them and that part of the donor layer which remains nonionized has to be computed numerically. Although we do neglect the small effect of different dielectric constants of GaAs and $Al_xGa_{1-x}As$, we do, however, fully include the image charges of the electrons and donors due to the potential boundary conditions at the surface. In our approach the occupations of the surface states in the split are determined assuming Fermi level pinning midgap and thermodynamical equilibrium with the electrons at the junction. In making these assumptions we follow the same conventions as in Refs. 3 and 4, but not the prescription in the original work of Laux *et al.* In some of our calculations the assumption of thermodynamical equilibrium is extended also to the donors, but it should be remembered that this condition may be experimentally difficult to achieve unless the measurements are performed a sufficiently long time after preparation of the sample, so that equilibration by capture and emission of electrons by the DX centers is guaranteed. We shall therefore also consider, as an alternative case, the behavior of the device when it is prepared so that the donor layer is fully ionized and compare the effects on the electron gas.

Our study will focus on the interpretation of general trends rather than on the behavior of a specific device, and on simplifying assumptions that reduce the numerical work. Therefore one point which will be studied in detail is the precise formulation of the factorization assumption implicit in most two-dimensional models: i.e., that the wave functions of the electrons can be approximated by the product of an in-plane component times a common component orthogonal to the plane of the junction. In Sec. III we will present a systematic way to implement this factorization and study its quantitative accuracy.

II. THE THREE-DIMENSIONAL MODEL

We study conventional heterojunction structures made of successive plane layers of GaAs and $Al_xGa_{1-x}As$, with

a metallic gate completely covering their surfaces except for a linear split. Starting at the exposed surface the devices consist of (i) a cap layer of GaAs of thickness c on top of which the metallic gate is deposited; the latter is maintained at a constant potential V_g and has a linear split of constant width w; (ii) a "donor" layer of $Al_xGa_{1-x}As$ of thickness d and n doped with a constant donor number density ρ_d; (iii) an undoped spacer layer made also of $Al_xGa_{1-x}As$ of thickness s; and (iv) an undoped substrate of GaAs whose thickness will be considered infinite for all practical purposes. Since these devices are translationally invariant in the direction defined by the split gate, it is convenient to choose this as the z axis, setting the origin at a point in the middle of the split, and in the orthogonal plane, choosing the x axis parallel to the surface and the y axis directed towards the inside of the semiconductor.

A. The electrostatic potential

The potential acting on the electrons in the device is due to a combination of charges at the surface, including those in the gates, to the ionized donors, and to the electrons in the junction. We will construct this potential taking into account successively all these sources of electric field. The potential $V_{sg}(x,y)$ generated by a split gate at potential V_g in the absence of other charges has to satisfy the Laplace equation everywhere in the half plane $y>0$ with the boundary condition

$$V_{sg}(x,y=0)=\begin{cases} V_g & \text{when} \quad |x|>w/2 \\ 0 & \text{when} \quad |x|<w/2. \end{cases} \tag{1}$$

The function fulfilling these conditions has already been written down by Davies:[8]

$$V_{sg}(x,y)=V_g\Big\{1-\frac{1}{\pi}\Big[\arctan\Big(\frac{w/2-x}{y}\Big)+\arctan\Big(\frac{w/2+x}{y}\Big)\Big]\Big\}. \tag{2}$$

Note that with this choice

$$\lim_{y\to\infty} V_{sg}(x,y)=V_g, \tag{3}$$

so that the electric field at infinity vanishes, as required by other authors who integrate the Poisson equation directly.

There are two other sources of potential in the device: the ionized donors and the electrons in the wire. Due to translation invariance along the wire axis, the infinitesimal elements contributing to the electrostatic field will be in both cases linear filaments parallel to the z axis with uniform linear charge density $\pm e\rho(x',y')\,dx'\,dy'$. (In our convention $e<0$ is the electron charge.) Each filament contributes a potential:

$$dV_f(x,y)=-\frac{\pm e}{4\pi\varepsilon}\rho(x',y')dx'dy' \times \ln[(x-x')^2+(y-y')^2] + \text{const}, \tag{4}$$

and this has to be summed over all elements with nonvanishing charge. However, adding these contributions directly to V_{sg} leads to a total potential that does not verify the boundary condition in Eq. (1). To satisfy that condition image charges must be added and each of the linear filaments above acquires an image filament with opposite charge located mirror symmetrically with respect to the surface.

Applying the above prescription to the charge densities $e\rho_e(x',y')dx'dy'$ leads to the Hartree potential acting on an electron due to the others:

$$V_e(x,y)=-\int_{y_2}^{\infty}dy'\int_{-\infty}^{\infty}dx'\frac{e\rho_e(x',y')}{4\pi\varepsilon} \times \ln\frac{(x-x')^2+(y-y')^2}{(x-x')^2+(y+y')^2}, \tag{5}$$

where $y_2\equiv c+d$. As we will show later, the additional effects due to exchange (Fock term) and e-e correlations are small, so we have used the Slater approximation for the Fock term and, following the classic work of Stern and Das Sarma,[9] the parametrization proposed by Hedin and Lundqvist[10] to include e-e correlations. The appropriate expressions can be found in these references and in an earlier work by us.[11]

A simpler case of application of this method of images is that of a fully ionized donor layer located in a slab: $c<y<c+d$, with uniform charge density $-e\rho_d$: the corresponding mirror slab is located at $-c-d<y<-c$, with density $e\rho_d$. Using the well known expressions for slabs with a uniform charge distribution one finds an electrostatic potential:

$$\begin{aligned} V_d(0<y<c)&=-\frac{e}{\varepsilon}\rho_d\,dy, \\ V_d(c\le y<y_2)&=-\frac{e}{\varepsilon}\rho_d[d\,y-\tfrac{1}{2}(y-c)^2], \\ V_d(y_2\le y)&=-\frac{e}{2\varepsilon}\rho_d\,d\,(2c+d). \end{aligned} \tag{6}$$

Note that these slabs produce a zero electric field in the substrate (also when $y\to\infty$), indicating that the charge in the donor layer has been fully compensated by an additional induced charge in the gates. The potential due to the gates and the donors is thus

$$V_{sg+d}(x,y)=V_{sg}(x,y)+V_d(y), \tag{7}$$

so that the total potential affecting the electrons is

$$V(x,y)=V_{sg+d}(x,y)+V_e(x,y). \tag{8}$$

We determine the conduction band edge by multiplying by the electron charge e and choosing an appropriate origin of energies. We follow the convention of fixing this origin at the energy of the bound surface states in the split and write $e\phi_s>0$ for the binding energy of these states with respect to the conduction band. The assumption of thermodynamical equilibrium between these states and the electron gas therefore sets the Fermi level at zero energy. Then the band edge is given by

$$eV(x,y)=e\phi_s+eV_{sg+d}(x,y)+eV_e(x,y)+eV_b\,, \tag{9}$$

where the last term accounts for the band offset between GaAs and $Al_xGa_{1-x}As$.

When the assumption of thermodynamical equilibrium is extended to the donors, the above expressions for $V_d(y)$ apply only when the donor layer is fully ionized, so that at all its points $eV(x,y) > e\Phi_i$, the latter being the ionization potential. When this is not the case, in those points where the previous condition is not met the donors remain neutral. We describe this situation by positing that in addition to a fully ionized donor layer at these points there is a compensating distribution of electrons. We then add to Eq. (9) the additional potential due to this latter charge distribution. In split-gate devices, the donor layer is always fully ionized below the gates, and there is at most a symmetric nonionized thin strip running parallel to the split. At $T = 0$ K that strip is characterized by a boundary, $x_b = \pm x_b(y)$, which has to be determined simultaneously with the other quantities during the self-consistent process. Assuming it to be known, then the additional contribution reads

$$\Delta V_d(x,y) = -\frac{e\rho_d}{4\pi\varepsilon}\int_c^{y_2} dy' \int_{-x_b(y')}^{+x_b(y')} dx' \times \ln\frac{(x-x')^2+(y-y')^2}{(x-x')^2+(y+y')^2}. \quad (10)$$

When $T \neq 0$ K we assign to each point (x',y') in the above integral a fractional occupancy according to the prescription

$$\nu_d(x',y') = \frac{1}{1+\exp\{[eV(x',y') - e\Phi_i]/k_BT\}} \quad (11)$$

and determine the boundary by selecting only those points for which ν_d is not negligibly small.

B. Pinch-off potential

We discuss here its determination for a fully ionized donor layer, leaving the partial ionization case for the next section. $V_{g,po}$ is the critical value of V_g for which the electron density at the junction vanishes. Ignoring quantal effects due to zero point motion, this requires that the bottom of the conduction band at the boundary between spacer and substrate should lie just at zero energy:

$$eV(x=0, y=y_3+0^+) = 0, \quad (12)$$

where $y_3 \equiv c+d+s$. From this it follows that

$$eV_{g,po} = \frac{\frac{e^2}{2\varepsilon}\rho_d d(2c+d) - e\phi_s}{1-\frac{2}{\pi}\arctan\left(\frac{w}{2y_3}\right)}. \quad (13)$$

As an example we consider a device, named L1 from now on, with the same physical parameters as that originally studied by Laux *et al.*: $c = 24$ nm, $d = 36$ nm, $s = 10$ nm, $w = 400$ nm, binding energy of surface states $e\phi_s = 0.7$ eV, $\rho_d = 0.0006$ nm^{-3}, conduction band offset $eV_b = 0.2$ eV, donor ionization energy $e\Phi_i = 0.05$ eV, and relative dielectric constant $\varepsilon_r = 13.1$. From Eq. (13) one then gets $V_{g,po} = -2.58$ V. However, as already pointed out by Davies,[8] due to zero point motion, a bound subband exists only for potential wells in the substrate whose depth is greater than a certain minimal value. The calculations that we will later show indicate that this minimal depth is of about $eV_{0pm} \simeq -0.064$ eV. To include this effect, the numerator of Eq. (13) has to be increased by that amount, and this leads to an improved estimate of $V_{g,po} = -2.28$ V. As we shall see, this estimate agrees well with the extrapolation of our self-consistent calculations to zero electron density. Since the interesting regime of work of a quantum wire is that of small electron densities, we shall be concerned with values of the gate potential only slightly above $V_{g,po}$. It was already remarked by Davies[8] that the different surface boundary conditions assumed here, Eq. (2), and in the original work of Laux *et al.*[1] lead to very different pinch-off potentials. As stated in the Introduction we have preferred to follow the more recent prescriptions of Refs. 3 and 4.

C. The electron wave functions and densities

Since the potential energy is independent of the z coordinate, in the envelope function approximation the wave functions of the electrons in the gas can be written in the factorized form

$$\Phi_{n,k_z}(x,y,z) = \frac{1}{\sqrt{2\pi}} e^{ik_z z}\Psi_n(x,y), \quad (14)$$

where n is the subband index and Ψ_n is a solution of the two-dimensional Schrödinger equation:

$$\left[-\frac{\hbar^2}{2m^*}\left(\frac{d^2}{dx^2}+\frac{d^2}{dy^2}\right) + eV(x,y)\right]\Psi_n(x,y) = E_n\Psi_n(x,y), \quad (15)$$

with boundary conditions that it vanishes at $y = y_2$, and also when $y \to \infty$ or when $x \to \pm\infty$. For convenience this wave function is normalized to unity. The subband occupations are determined by

$$\nu_n = \frac{1}{\pi}\sqrt{\frac{2m^*k_BT}{\hbar^2}}\, F_{-1/2}\left(-\frac{E_n}{k_BT}\right), \quad (16)$$

where $F_{-1/2}$ is the Fermi-Dirac integral, as in Refs. 4 and 5, and it should be remembered that in our convention the Fermi level is set at zero energy. Thus

$$\rho_e(x,y) = \sum_n \nu_n\, |\Psi_n(x,y)|^2, \quad (17)$$

and the sum is truncated when the ν_n becomes negligible. For later use we define explicitly the two-dimensional and linear densities as

$$\sigma(x) = \int_{y_2}^{\infty} \rho_e(x,y)\, dy, \qquad \lambda = \int_{-\infty}^{\infty} \sigma(x)\, dx. \quad (18)$$

The dependence of $\rho_e(x,y)$ and $eV(x,y)$ on each other, explicit in the above expressions, requires use of an iterative method for their determination. This self-consistent process consists of (i) starting with some trial $V_e(x,y)$, to construct the total potential $V(x,y)$, (ii) solving the Schrödinger equation, Eq. (15), for the occupied subbands and constructing $\rho_e(x,y)$, (iii) with that charge density, computing $V_e(x,y)$ from Eq. (5), determining $x_b(y)$ and ν_d, constructing $V(x,y)$, and returning again to step (ii) until the results converge.

We solve the two-dimensional Schrödinger equation, (15), using a rectangular mesh defined in the spacer and substrate: $|x| < x_m$, $y_2 < y < y_m$, with boundary conditions such that its solutions vanish on the sides of that rectangle. Typical values for device L1 are $x_m \leq 100$ nm, $y_m = y_2 + 35$ nm. Since the potential is symmetric under the exchange $x \to -x$, the wave functions Ψ_n have a definite parity under that transformation and the explicit calculation can be restricted to $x \geq 0$ with boundary conditions now chosen according to the symmetric or antisymmetric character of each wave function. Because we are interested only in determining the subbands close to the Fermi energy, i.e., only a few of the lowest eigenvalues and their eigenfunctions, the Lanczos algorithm is well suited to the purpose. This method allows one to reformulate the matrix problem that results from discretization in the above mesh into one of finding the eigenvalues of a tridiagonal matrix. When only the lowest eigenstates are needed, this matrix can be truncated sizably without losing much accuracy. We followed the method as described in Refs. 12. In instances where the Lanczos algorithm failed to produce sufficiently accurate results we improved on them by performing inverse iteration, as described in Sec. 11.7 of *Numerical Recipes*.[13] The accuracy of the results was tested using two-dimensional separable potentials (linear in y and harmonic oscillator, square well or stretched harmonic oscillator in the x coordinate). For the computation of the Hartree potential acting on the electrons the same mesh was used. The calculation of the double integrals was found to be much less time consuming than the solution of the differential equation. The numerical code is run on a 486DX-33 PC and typical running times per iteration are less than 2 min.

D. Results

For simplicity we shall show first results for device L1 at $T = 0$ K and with the donor layer fully ionized. As will be seen later, at low T the donor layer of this device is only partially ionized in thermodynamical equilibrium, so that in experiment this full ionization condition could only be attained by photoionization or by cooling under a suitable negative bias.

The most representative results of the self-consistent calculation are summarized in Figs. 1–4. The continuous line in Fig. 1 shows the variation of the linear electron density, Eq. (18), with gate potential. As can be seen, the results extrapolate well to the pinch-off value derived above. The corresponding two-dimensional densities are shown in Fig. 2. [Only the values for positive x are shown since $\sigma(x)$ is symmetric.] The lowest subband energies are plotted in Fig. 3, again as a function of the gate potential. And in Fig. 4 the potential as a function of x for $y = y_3 + 6$ nm is shown also for several V_g. This value of y was chosen because it is where the electron density peaks. We shall not dwell on these results because they are qualitatively similar to those already found by other authors. These figures will also be used to gauge the quality of the "two-dimensional" approximation to be presented in the next section.

For a better understanding of the connection between the changes in V_g and those of the results just shown, the variation of the potential and the wave functions with depth has to be analyzed: for two selected values of V_g we

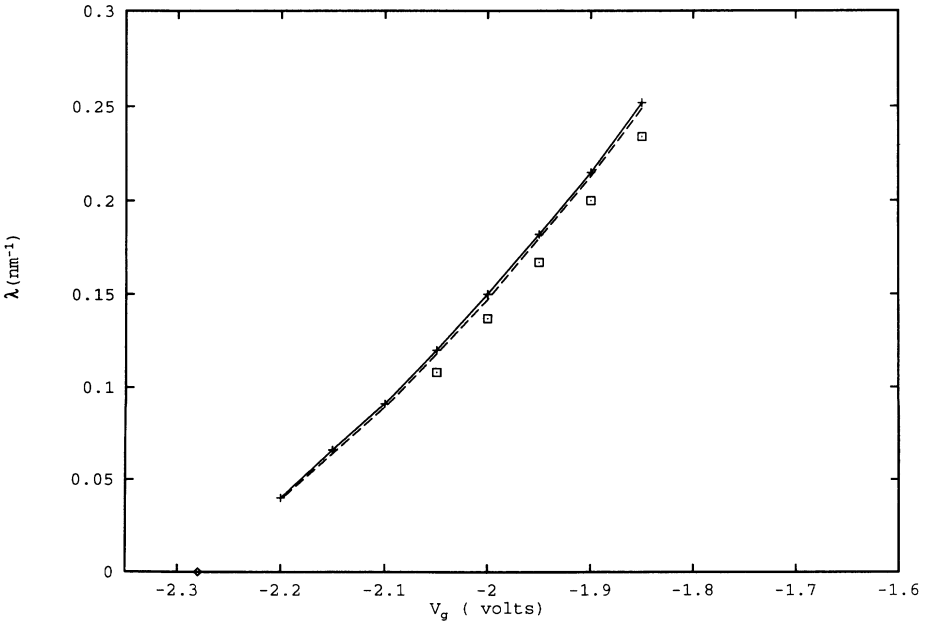

FIG. 1. Linear densities for various gate potentials, fully ionized donor layer. Continuous line: three-dimensional calculation; dashed line: two-dimensional approximation; squares: prediction omitting the exchange and electron correlation terms. Diamond on the x axis: pinch-off potential.

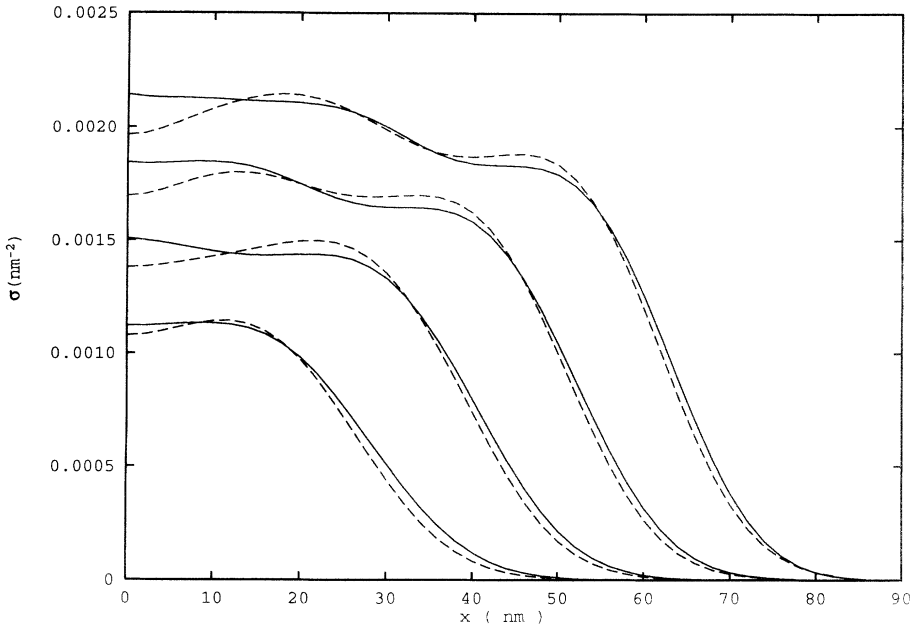

FIG. 2. Two-dimensional densities, $\sigma(x)$, for gate potentials $V_g = -1.85, -1.95, -2.05$, and -2.15 V from top to bottom. Continuous lines: 3D calculation; dashed lines: 2D approximation.

show in Fig. 5 the gates plus donors potential, eV_{sg+d} and the full potential, eV, as a function of y, with $x = 0$ fixed. It is seen that the repulsive Hartree potential pushes up the conduction band edge in both cases, by an amount that *on the scale of the figure* renders the two curves for the total potential almost indistinguishable. The same is found for other values of V_g. This shows that there is a large compensation between the changes in eV_{sg+d} induced externally by varying V_g, and those produced in the Hartree potential by the increase in the density of electrons. Plotting $eV(x, y)$ we have found that systematically the slope of the walls responsible for confinement in the x direction is lower than the slope in the y direction shown in Fig. 5. Since the Coulomb potential is long ranged, the Hartree term varies quite smoothly in the rectangular domain of substrate and spacer of nonvanishing electron density, and the qualitative features of the slopes of the confining walls are those of eV_{sg+d} so that they can be easily studied, even with analytical approximations. The changes in density can be qualitatively understood using a Fermi gas model for the electrons. When the gate potential is lowered in absolute value, eV_{sg+d} is also lowered in the substrate, as shown in Fig. 5, and this favors an increase in the electron density.

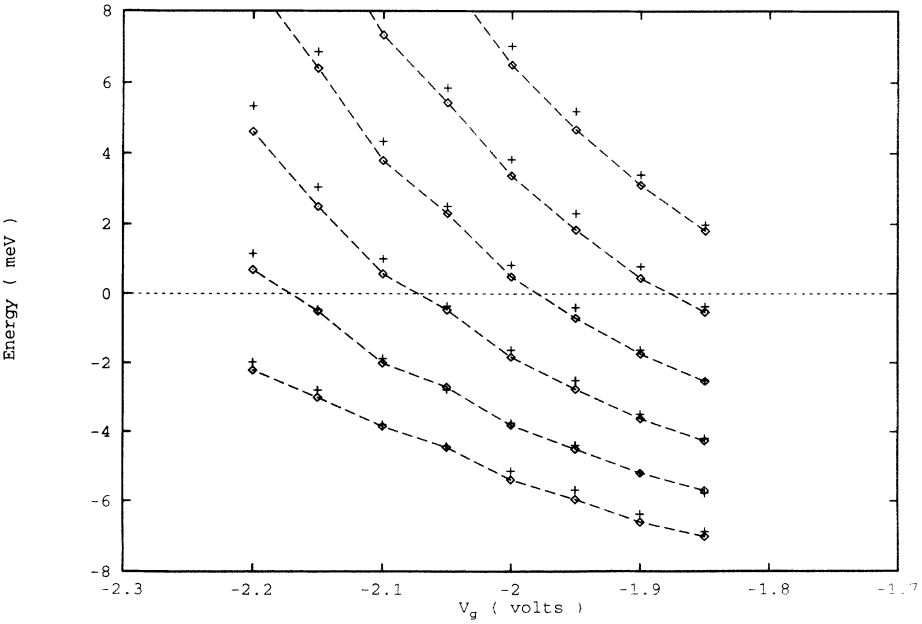

FIG. 3. Variation of lowest subband energies with gate potential. Dashed line with diamonds: 3D calculation; crosses: 2D approximation.

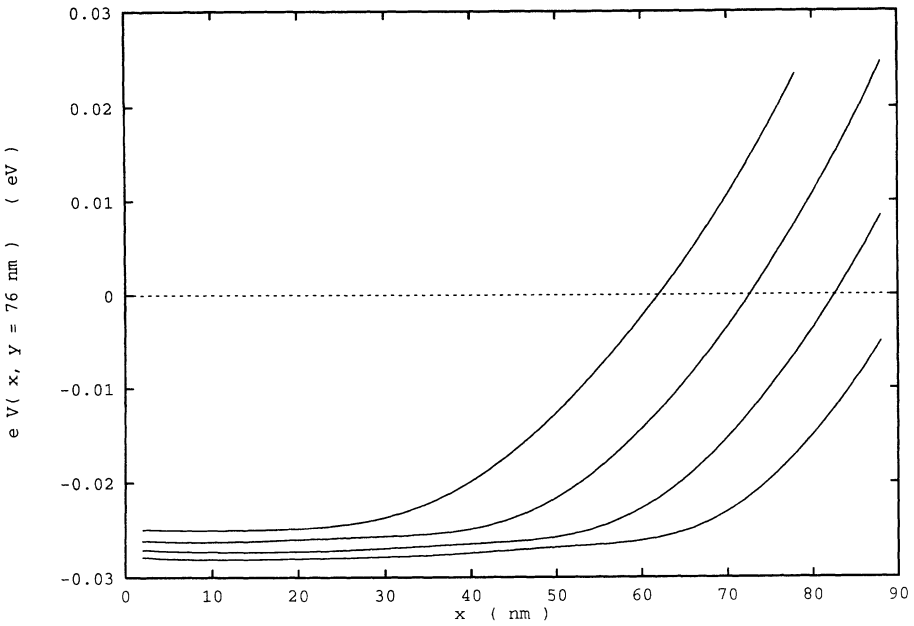

FIG. 4. Total potential, $eV(x,y)$, for fixed $y = 76$ nm and the same four values of V_g as in Fig. 2, now from bottom to top.

This tendency is partially compensated by the increase in the Hartree potential. Since the confining walls are less steep in the x than in the y direction the electron density finds it much easier to grow by expanding laterally; precisely the trend seen in Fig. 2.

The changes in Fig. 4 can also be interpreted qualitatively: For a fixed y, the variation with x of the Hartree term is found to have a shape reminiscent of a Gaussian: it is maximal and slowly varying at small x and starts to decrease smoothly roughly at the same x where $\sigma(x)$ also does. Since the potential eV_e can be viewed as the convolution of the electron density with the screened Coulomb potential between point charges it will tend to the shape of $\sigma(x)$, but smoothed by the convoluting function. Since the latter is long ranged this makes the decrease very slow. The variations of eV_e nearly compensate those of eV_{sg+d} at small x, so that, as shown in Fig. 4, $eV(x, y = 76\text{ nm})$ is almost constant at small x. In the larger scale of the figure one can see, however, that the compensation between these changes found in Fig. 5 is not complete, and that the bottom of the confining potential descends when the absolute value of the gate potential decreases. This explains the increase in the central values of $\sigma(x)$ found in Fig. 2.

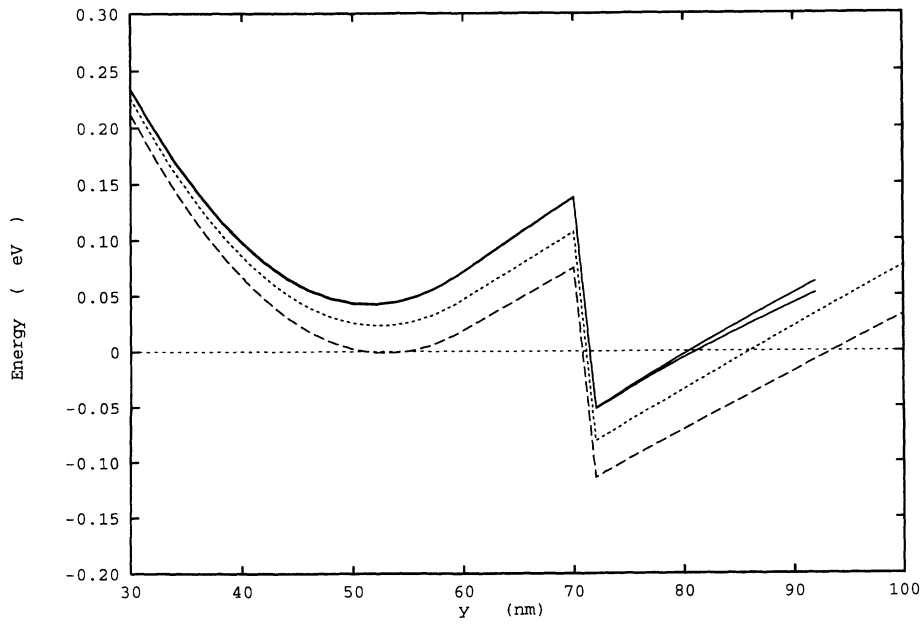

FIG. 5. Total and gates plus donors potentials for fixed $x = 0$ as a function of y. Continuous lines: $eV(0,y)$; dashed lines: $eV_{sg+d}(0,y)$. Short dashes correspond to $V_g = -2.10$ V, long dashes to $V_g = -1.95$ V.

Figure 5 also shows the well known quasilinear variation of the potential in the substrate. Clearly the slope of that variation depends on the gate potential. To examine this point further we have fitted straight lines to the curves $eV_{sg+d}(0,y)$ and $eV(0,y)$ in the substrate. We have found that for a given V_g the slopes of the total potential and of eV_{sg+d} are very close: their difference is negligible near pinch off and grows to $\simeq$ 3% when $V_g = -1.9$ V. This is again a consequence of the smoothness of the variation of the Hartree term and will support the approximation to be described in the next section.

The basis of the models that treat the electron gas at the junction as two dimensional is the assumption that it is a good approximation to factorize the subband wave functions as

$$\Psi_n(x,y) \simeq \Psi_n^{\mathrm{mod}}(x,y) \equiv \phi_n(x)A(y)\,, \tag{19}$$

where the two functions in the right-hand side are taken to be separately normalized. It is immediately verified that in this approximation the ratio

$$r(x,y) \equiv \sqrt{\frac{\rho_e(x,y)}{\sigma(x)}} \tag{20}$$

should be equal to $A(y)$ and thus be independent of x. In Fig. 6 we have plotted the ratio $r(x,y)$ obtained from our self-consistent $\rho_e(x,y)$ and $\sigma(x)$, at the points of the rectangular mesh used to solve the Schrödinger equation. The continuous line shows the curve that corresponds to the average over x of the values for a fixed y vs y and the vertical "error bars" at each point indicate the extreme values of the ratio. The smallness of these error bars shows that this ratio is to a good approximation independent of x, thus supporting the factorization approximation. However, as shown in the same figure, the profile of the $A(y)$ thus extracted is different from that of a truncated Airy function, mainly due to tunneling into the spacer layer. The latter is constructed so that (i) its zero is located at the boundary between spacer and substrate, and (ii) it corresponds to a linear potential whose slope (0.0058 eV/nm) is an average of that of the curves $eV(0,y)$ in the substrate. We have found that for all V_g considered the $A(y)$ are similar, but close examination shows, as expected, that as the slope of $eV(0,y)$ decreases the $A(y)$ expand slightly towards large y. This trend is much better seen in the wave function for the "extreme" case $V_g = 0$ (ungated device), taken from Ref. 11, also shown in the figure: whereas the tunneling into the spacer remains similar, one sees that under the effect of the negative potential the electron gas becomes much more concentrated at the junction.

We have examined the effect of the contributions due to exchange and e-e correlations, included in the Hedin-Lundqvist approximation. The Fock term is of opposite sign to the Hartree potential and is therefore attractive for electrons. Its contribution thus lowers the potential in the substrate and produces an increase in the electron density. Since in the Slater approximation the exchange potential is proportional to $\rho_e^{1/3}$ the effect of this term increases with λ. But, as can be seen in Fig. 1, it is comparatively small even for the largest of the linear densities considered. The changes in $\sigma(x)$ are also small and what is qualitatively more important is the slight smoothing of the decrease of the density at large x when these terms are omitted. The additional effect of the e-e correlations that we find is even smaller, practically negligible on the scale of these figures.

E. Finite temperatures

We have studied the systematic changes produced by increasing the temperature up to 50 K, keeping the as-

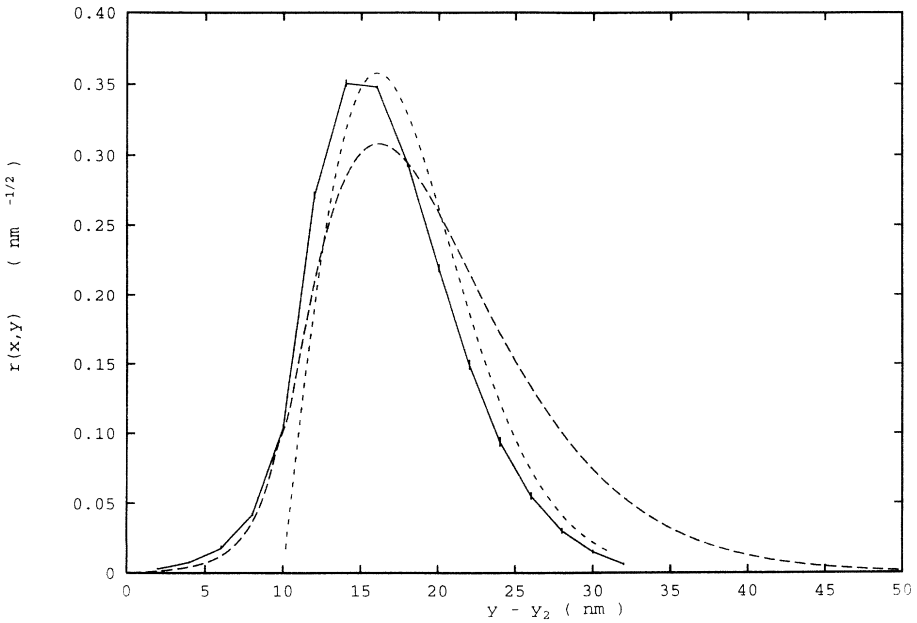

FIG. 6. Continuous line: average over x of the ratio $r(x,y)$ defined in Eq. (20). The vertical bars connect the extreme values of the ratio at the chosen y values. Long dashed line: wave function for the ungated device. Short dashed line: normalized function corresponding to a linear potential with an infinite wall at the junction.

sumption of a fully ionized donor layer. The changes are small and go in the expected directions: as shown in Fig. 7, due to the spread of the occupations over a larger set of subbands, the two-dimensional densities expand and progressively become smoother, with less pronounced oscillations in their inner part and a slower decrease to zero. The changes in the total linear density are very small: for the case considered in the figure, $V_g = -2.00$ V, the increase in λ when T rises from 0 to 50 K is of only $\simeq 6\%$. The changes in the subband energies are more significant, as shown in the inset in Fig. 7, where it is seen that the increases in T push them upwards, a change related to the increase in λ. Similar changes are found for other gate potentials. We therefore conclude that in this domain of temperatures there are no qualitatively significant changes in the bulk properties of the device.

F. Donor layer partially ionized

As already pointed out, under the assumption of thermal equilibrium, and when the value chosen for the ionization potential is $e\Phi_i = 0.05$ eV, a part of the donor layer below the split in the gate remains neutral. As described in Sec. II, there is then an additional piece in the contribution of the donor layer to the electrostatic potential that accounts for the repulsion between the electrons retained in this layer and those in the gas.

As a representative case we have chosen to study the same device L1 as before, at $T = 20$ K, but now assuming that the occupations in the donor layer are determined by the thermodynamical equilibrium condition. The linear densities for several V_g are shown in Fig. 8, together with the corresponding linear densities of electrons trapped in the donor layer. Taking as reference the case previously studied, Fig. 1, the changes in the linear densities are quite important. The two-dimensional densities for the two cases, when $V_g = -2.00$ V, are shown in Fig. 8 (inset): due to the smallness of the spacer layer (remember that $s = 10$ nm), the electrons trapped at the donor layer generate a rather strong repulsive potential everywhere in the junction, with the repulsion being maximal near $x = 0$, so that σ is reduced in magnitude everywhere. A two-dimensional plot of $eV(x, y)$ shows, as expected, that the additional repulsive potential is stronger near the center of the wire and closer to the junction. This is reflected in the subband energies: while the lowest, and thus with a wave function maximal at the middle of the wire, increases by some 2.0 meV, for the sixth subband the increase is only some 1.7 meV. However, these changes have a very simple interpretation: some of the electrons that were previously in the gas have now moved to the zone of the minimum in the conduction band edge in the donor layer, making it rise until the energy of the electrons trapped by the donors equals that of the Fermi level in the gas. It is interesting that the sum of linear densities at the donor layer and the junction is now close ($\simeq 15\%$ higher) to the linear density found for the same V_g in the full ionization case. Again this is a consequence of the smoothness and long range of the mean field created by the electrons and of the smallness of the spacer layer: the total Hartree potential in the substrate is not too different when part of the electrons in the gas are transferred to the donor layer, and therefore the total amount of charge does not need to change much to fulfill the equilibrium conditions.

The same *conservation* mechanism operates when we study the changes produced when the Coulomb exchange terms are suppressed: this increases the repulsion in the substrate and, as can be seen in Fig. 8, there is an additional transfer of electrons to the donor layer that leaves the total linear density almost unchanged. Note also that, as can be seen again in Fig. 8 extrapolating to

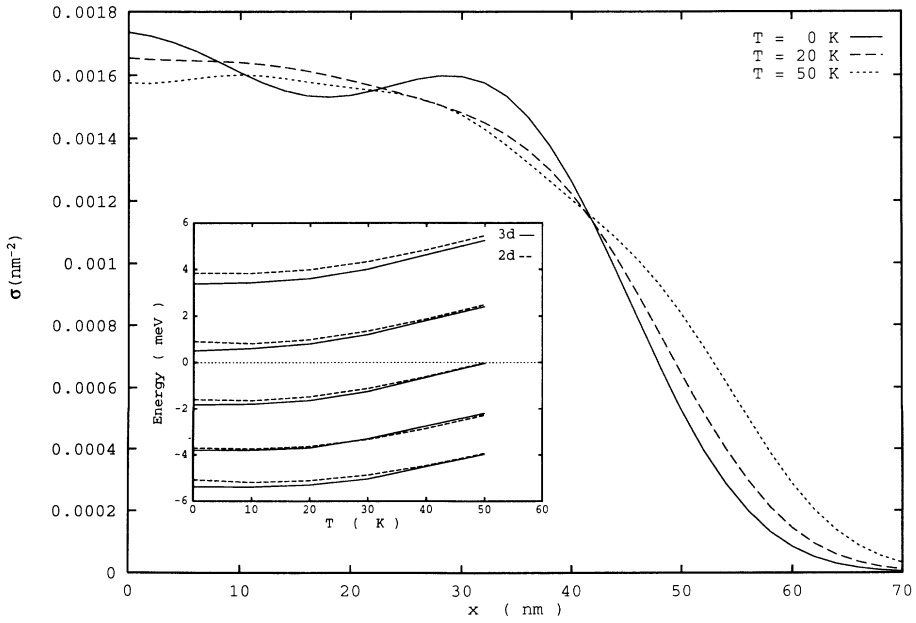

FIG. 7. Variation with temperature of the two-dimensional density corresponding to $V_g = -2.00$ V. Three-dimensional calculation assumes a fully ionized donor layer. Inset: Variation of subband energies. Continuous line: 3D calculation; dashed line: 2D approximation.

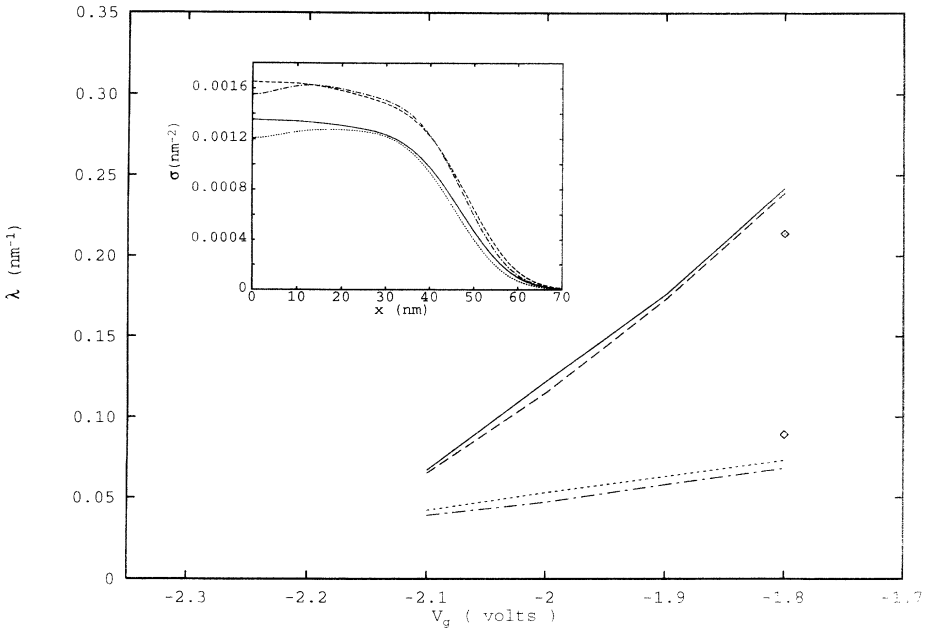

FIG. 8. Linear electron densities at the gas and donor layers; 3D gas, solid line; 2D gas, dashed line; 3D donor, dash-dotted line; 2D donor, dotted line. The diamonds are the results of 3D calculations for $V_g = -1.8$ V, omitting the Coulomb exchange contribution. Inset: Comparison of $\sigma(x)$ for fully and partially ionized donor layer cases. $V_g = -2.0$ V and $T = 20$ K. Partial ionization: continuous line, 3D model; dotted line, 2D model. Full ionization: dashed line, 3D model; dot-dashed line, 2D model.

zero linear density, the pinch-off potential for this partial ionization case is slightly shifted to smaller $|V_g|$ with respect to that in Fig. 1, again in accordance with the above transfer process.

We finally stress that this sizable dependence of the density of electrons in the gas on the degree of ionization of the donor layer implies that a meaningful comparison between theoretical predictions and experiment will only be possible when the conditions under which the device is prepared and the experiment is performed are carefully controlled.

III. THE TWO-DIMENSIONAL MODEL

In the preceding section we have seen that the factorization of Eq. (19) is a good approximation provided that for each value of V_g the appropriate $A(y)$ is constructed, taking into account the tunneling into the spacer and the variation of slope of $eV(x,y)$ with y when V_g is varied. We shall now present a systematic way of implementing the factorization approximation which incorporates these effects and therefore reproduces very accurately the trends found in our more exact calculations. The first step consists in rewriting the Schrödinger equation, Eq. (15), as

$$\left[-\frac{\hbar^2}{2m^*}\left(\frac{d^2}{dx^2}+\frac{d^2}{dy^2}\right)+eV_{sg+d}(0,y)+[eV(x,y) - eV_{sg+d}(0,y)]\right]\Psi_n(x,y) = E_n\Psi_n(x,y), \quad (21)$$

and then approximate $eV(x,y) - eV_{sg+d}(0,y)$ by a weighted average over y: we define

$$U(x) \equiv \int_{y_2}^{\infty} A^2(y)\,[eV(x,y) - eV_{sg+d}(0,y)]\,dy\,, \quad (22)$$

with a normalized weight function, $A(y)$, to be chosen in a moment. This leads to approximating Eq. (21) by

$$\left[-\frac{\hbar^2}{2m^*}\left(\frac{d^2}{dx^2}+\frac{d^2}{dy^2}\right)+eV_{sg+d}(0,y)+U(x)\right]\Psi_{n,a}(x,y) = E_{n,a}\Psi_{n,a}(x,y), \quad (23)$$

which is separable into

$$\left(-\frac{\hbar^2}{2m^*}\frac{d^2}{dy^2}+eV_{sg+d}(0,y)\right)A(y) = E_a^{(y)}A(y) \quad (24)$$

and

$$\left(-\frac{\hbar^2}{2m^*}\frac{d^2}{dx^2}+U(x)\right)\phi_n(x) = E_{n,a}^{(x)}\phi_n(x)\,, \quad (25)$$

with

$$\begin{aligned}\Psi_{n,a}(x,y) &= \phi_n(x)A(y),\\ E_{n,a} &= E_a^{(y)} + E_{n,a}^{(x)},\\ U(x) &= U_{sg+d}(x) + U_e(x)\,.\end{aligned} \quad (26)$$

The different pieces of this potential have the explicit forms

$$\begin{aligned}U_{sg+d}(x) &= -\frac{V_g}{\pi}\int_{y_2}^{\infty} A^2(y)\left[\arctan\left(\frac{w/2-x}{y}\right)+\arctan\left(\frac{w/2+x}{y}\right)-2\arctan\left(\frac{w}{2y}\right)\right]dy,\\ U_e(x) &= -\frac{e^2}{4\pi\varepsilon}\int_{y_2}^{\infty} A^2(y)dy\int_{-\infty}^{\infty}dx'\int_{y_2}^{\infty}dy'\ln\frac{(x-x')^2+(y-y')^2}{(x-x')^2+(y+y')^2}\,\sigma(x')A^2(y')\,,\end{aligned} \quad (27)$$

and a third contribution, $\Delta U_d(x)$, obtained similarly from Eq. (10), to be added in the case of partial ionization of the donor layer. The two-dimensional density is now constructed directly as

$$\sigma(x) = \sum_n \nu_n |\phi_n(x)|^2, \tag{28}$$

with the ν_n already defined in Eq. (16). This set of equations (24)–(28) summarizes the simplification accomplished: the two-dimensional wave functions now factorize into a common y-dependent function, $A(y)$, which is determined once and for all by solving Eq. (24), and an x-dependent part that has to be determined iteratively. Note that the integrations over y and y' in Eqs. (27) need be done only once, so that the whole iterative process refers only to x-dependent functions. The numerical solution of the one-dimensional Schrödinger equations is now straightforward and very fast, and the construction of the different pieces of $U(x)$ requires also only one-dimensional integrations, except for the piece $\Delta U_d(x)$. The whole iterative process is much faster than that described in the preceding section. Note, however, that since $eV_{sg+d}(0,y)$ depends on V_g, the weighting functions $A(y)$ are different for each gate potential, so that the above approximation accounts better for the changes of the external potential than would a cruder model in which a universal form for $A(y)$ is imposed from the beginning. This would be the case, e.g., if we had made the ansatz of choosing $A(y)$ proportional to a truncated Airy function.

Results

The predictions of this approximation have already been shown in most of the figures presented for the three-dimensional calculations and by now it should be clear that the two-dimensional model is quite successful in all cases considered: fully or partially ionized donor layers and different temperatures, not only qualitatively, but also quantitatively to a high degree of accuracy. It is therefore a very useful tool in the study of all these systematic changes.

When the different contributions defined in the approximation process are considered separately the final agreement found is surprisingly good. Let us consider as an example the prediction for the occupations ν_n. For the particular case $T = 0$ K and for states below the Fermi level (remember that $E_F = 0$ in our convention), Eq. (16) reduces to

$$\nu_n = \frac{2}{\pi}\sqrt{-\frac{2m^* E_n}{\hbar^2}}\,. \tag{29}$$

The E_n are now given by Eq. (26) as the difference of two large terms: e.g., for $V_g = -2.0$ V and a fully ionized donor layer we find $E_{1,a} = -67.10 + 61.97 = -5.13$ meV. The agreement found in Fig. 3 for the subband energies and that in Figs. 1 and 2 for the densities is critically dependent on an accurate prediction by the two-dimensional (2D) model of these two large terms. As has been stressed when discussing Fig. 5, the Hartree term gives a large contribution. It is the fact that it is sufficiently smooth that makes the replacement of the y dependence of $eV(x,y)$ by that of $eV_{sg+d}(x,y)$ sufficiently accurate for the determination of a good $A(y)$. In devices whose geometry induces more rapidly varying Hartree contributions one should then expect the 2D model to become less accurate, and cause the electron gas to depart from behaving as a two-dimensional system.

IV. SUMMARY AND CONCLUSIONS

We have presented a self-consistent approach to the potential energy of electrons in a linear split-gate heterojunction device. Solution of the Poisson equation has been simplified by following Davies's method[8] to account for the gate potential and surface boundary conditions. Further, we have studied the accuracy of the commonly used two-dimensional approximation to the full three-dimensional system. Our formulation for this approximation is shown to be very accurate, and simple to carry out. As a result, one can make systematic studies with little computational effort.

Work is in progress to formulate a two-dimensional Thomas-Fermi approximation for the electron gas at the junction based on the above results. We have found that a Thomas-Fermi approximation for the three-dimensional case fails badly in reproducing the shape of $A(y)$ and although the results for the linear densities show the same qualitative trends as above they are not quantitatively accurate. Results for these models will be presented in a future publication.

ACKNOWLEDGMENTS

We are grateful to NSERC Canada for continued support under Research Grant No. OGP00-3198 (D.W.L.S.). The work of J.M. is supported under Grant No. PB91-0236 of DGICYT, Spain.

[1] S. E. Laux, J. D. Franck, and F. Stern, Surf. Sci. **196**, 101 (1988).
[2] A. Kumar, S. E. Laux, and F. Stern, Appl. Phys. Lett. **54**, 1270 (1989).
[3] A. Kumar, S. E. Laux, and F. Stern, Phys. Rev. B **42**, 5166 (1990).
[4] G. L. Snider, I.-H. Tan, and E. L. Hu, J. Appl. Phys. **68**, 5922 (1990).
[5] T. Kerkhoven, A. T. Galick, U. Ravaioli, J. H. Arends, and Y. Saad, J. Appl. Phys. **68**, 3461 (1990).

[6] D. Jovanovic and J. P. Leburton, Phys. Rev. B **49**, 7474 (1994).
[7] Zhiqiang Wu and P. Paul Ruden, J. Appl. Phys. **74**, 6234 (1993).
[8] J. H. Davies, Semicond. Sci. Technol. **3**, 995 (1988).
[9] F. Stern and S. Das Sarma, Phys. Rev. B **30**, 840 (1984).
[10] L. Hedin and B. I. Lundqvist, J. Phys. C **4**, 2064 (1971).
[11] J. Martorell and D. W. L. Sprung, Phys. Rev. B **49**, 13 750 (1994).
[12] P. Hoodbhoy and J. W. Negele, Nucl. Phys. **A288**, 23 (1977); T. Sebe and J. Nachamkin, Ann. Phys. (N.Y.) **51**, 100 (1969).
[13] W. H. Press, B. P. Flannery, S. A. Teukolsky, and W. T. Vetterling, *Numerical Recipes* (Cambridge University Press, Cambridge, England, 1989).